Journal of Microelectronics and Electronic Packaging (2024) **21**, 35–41

ISSN: 1551-4897

Unlocking the True Power of Additive Manufacturing for EMI Shielding

Markus G. Scheibel,[1] Michael P. Kaiser,[2] Sutharsan Balasubramaniam,[2] Mykola Chernobryvko,[2] Julia-Marie Köszegi,[2] Marc Dreissigacker,[2] Marius Adler,[2] Tanja Braun,[2] Chuan I. Eric Huang,[1] Meng Jason Li,[1] Muriel Thomas,[1,*] and Franz Vollmann[1]

***Abstract*—Miniaturization trends in electronic packaging led to reduced spacing of individual packages on the printed circuit boards and thus increased the overall electromagnetic interference (EMI) levels within a device. State-of-the-art conformal coatings as EMI shielding layers are typically applied via sputter technology and offer design limitations with respect to coating selectivity on individual positions of the overall package. Our new technology of additively Ag layer application via inkjet printing overcomes today's design limitations and is a key enabler for next-generation packaging designs. In this study, we compare the shielding effectiveness (S.E.) on specifically designed transmission line emitter samples coated with state-of-the-art sputtered conformal layers against silver coatings applied via inkjet printing of particle-free metal-organic decomposition inks to evaluate the new technology for its potential on package-level shielding performance. Mechanical and electrical characterization of the silver coatings indicates appropriate tools to specify layer characteristics and ensure S.E. of 40 dB or higher at frequencies of 800 MHz and higher. The suitability of our well-tailored silver coatings to match typical S.E. requirements is shown with even much thinner layer thickness as compared with state-of-the-art coatings.**

***Keywords*—Printed electronics, inkjet printing, EMI shielding, 5G, system in package, package-level shielding**

Introduction

The miniaturization trends in printed circuit board (PCB) design and advanced semiconductor packaging have been proceeding for decades. As a result, the spacing between the individual packages decreases drastically and thus the electromagnetic noise within the electronic device increases, accordingly [1-6]. To prevent degradation in device performance or even failure, the initial approach of shielding enclosures was replaced successively by board-level shielding and later package-level shielding. The number of shielded devices increases just as much as the requirements for total shielding effectiveness (S.E.) [7, 8].

The manuscript was received on January 12, 2024; revision received on March 1, 2024; accepted on March 18, 2024.

The original version of this paper was presented at the 56th International Symposium on Microelectronics (IMAPS'2023), San Diego, CA, USA, October 3-5, 2023.

[1]Heraeus Printed Electronics GmbH, Heraeusstr. 12-14, Hanau, Germany
[2]Fraunhofer-Institute for Reliability and Micro integration, Gustav-Meyer-Allee 25, Berlin, Germany
*Corresponding author; email: muriel.thomas@heraeus.com

A typical example of a package, that is strongly affected by electromagnetic interference (EMI), is a system in package. These kinds of subassemblies commonly consist of a glass fiber reinforced substrate (i.e., FR4) carrying the semiconductors and covered by a molding cap of an electromagnetically transparent epoxy molding compound (EMC). The EMC cap is typically overcoated with a conformal coating that serves as the EMI shielding layer. The electrically conductive structure acts as a Faraday cage and inhibits the propagation of electromagnetic radiation in a range from several hundreds of MHz up to ≥6 GHz for 5G applications. The shielding layer is grounded by a connection to the substrate's reference plane that enables the shielding functionality.

Beyond the application for EMI management, conductive coatings are exploited in the context of hardware security to prevent and/or detect physical attacks on ICs [9].

Today's shielding layers are typically conformal coatings applied using gas phase deposition technologies such as physical vapor deposition or sputtering and build-up layers of two alternating steel use stainless (SuS) layers, and a center Cu layer in typical thicknesses of SuS/Cu/SuS of 2/4/2 μm or .18/3.8/.18 μm, respectively.

New trends in electronic packaging raise the requirements for more selective coatings and go beyond current design limitations originating from unselective shielding layer application methods. The electronic systems of the next decade demand a new generation of shielding technology. Additive manufacturing is a prime candidate to meet these needs.

Additive manufacturing technologies, such as inkjet-printed electronics of silver inks, gain increasing interest in the selective application of functional coatings, such as conductive layers.

Heraeus developed a turnkey solution for particle-free metal-organic decomposition (MOD) silver inks, well-tailored processes, and dedicated printing equipment. Fully integrated software converts application-specific layouts into process parameters to selectively place the individual ink-jetted droplets (drop-on-demand) on the individual substrates in a 2.5D topology, that are positioned on a wafer ring. The inkjet application method offers advantages of up to 99% material efficiency, layout flexibility (layout pattern and aspect ratio), rapid design changes during mass manufacturing, and a reduced number of process steps for masking (Fig. 1). Additionally, the process is ready for lights-off factory and allows for live monitoring of all relevant production and quality parameters during operations.

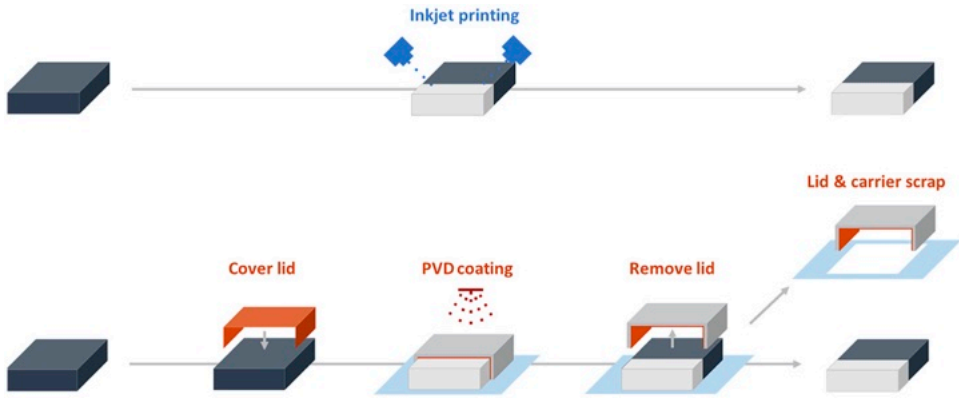

Fig. 1. Prexonics® inkjet printing offers customized selective printing (top) and sputtering or spray coating requires masking to create selective coating (bottom).

This full system solution ensures a long open time (∼1 month) on the printer and provides a coating technology that can easily tailored to each individual package design by adjusting the digital printing profile in the printer software. However, coating layer specifications for the quality assurance of conformal EMI shielding layers are still limited to experienced values derived from sputter technology and ignore the performance potential of selective coating technologies.

Within this study, we extract the S.E. performance of selectively applied silver coatings by inkjet printing on specifically designed transmission line packages and compare them against state-of-the-art sputtered samples. Mechanical and dielectric characterizations of silver coating layers will provide a fundament for the characterization and specification of such layers as the basis for quality assurance requirements. The respective sample layouts and testing characteristics will be described, and a principal overview of basic S.E. theory will be given.

Shielding by Inkjet-Printed Ag Coating

A. EMI Shielding

In general, there are three different mechanisms that contribute to EMI shielding. Each describes one interaction of electromagnetic waves at a material interface with different magnetic and dielectric properties:

1. Absorption A (dB)
2. Reflection R (dB)
3. Multireflection M (dB)

The electromagnetic wave can be absorbed by inducing currents in the conductive shielding materials that are removed via the grounding of the coating and result in an attenuation of the incoming wave longitudinal over the penetration depth (δ). The penetration depth

$$\delta = \sqrt{\frac{\rho}{\pi f_0 \mu_r \mu_0}} \tag{1}$$

depends on the frequency (f_0) of the absorbed wave, the resistivity of the shielding layer (ρ), its relative permeability (μ_r), and the vacuum permeability (μ_0). The absorption is the dominant shielding mechanism at high frequencies. At low frequencies, the skin depth is increasing, and a comparatively high shielding layer thickness must be realized for sufficient attenuation via absorption. The absorption term can be calculated by eq. (2).

$$A(\text{dB}) = 20\log\left|e^{\frac{t}{\delta}}\right| \tag{2}$$

Reflection, as the second shielding mechanism, occurs at the interface of two media with different wave propagating properties, namely a different intrinsic wave impedance η. The wave impedance is a function of magnetic permeability (μ) and dielectric permittivity (ε). A plane wave traveling in free space experiences the impedance of

$$\eta_0 = \sqrt{\frac{\mu_0}{\varepsilon_0}} = 377\ \Omega \tag{3}$$

Within a nonconductor, the impedance η_{NC} is determined by the permeability and permittivity of the respective material

$$\eta_{NC} = \sqrt{\frac{\mu_0 \mu_r}{\varepsilon_0 \varepsilon_r}} \tag{4}$$

and for conductors, η_C is dependent on the frequency of the incoming wave and on the electrical conductivity of conducting materials in addition.

$$\eta_C = \sqrt{\frac{2\pi f \mu_r}{\sigma}}. \tag{5}$$

The overall reflectance term for S.E. is given by the ratio of the intrinsic wave impedance at the interface between nonconductor and conductor and can be calculated according to

$$R(\text{dB}) = 20\ \log\frac{\eta_0}{4\eta_S}. \tag{6}$$

Finally, the fraction of the incoming wave, i.e., neither initially reflected at the surface of the shielding nor dissipated within the shielding can be reflected multiple times at the interfaces of shielding material and e.g., air. As a result, the effectiveness of the shielding is decreased. This multireflection plays an important role, particularly for low frequencies and thin shielding layer thicknesses (t), eq. (7).

$$M = 20\ \log\left|1 - e^{-2\frac{t}{\delta}}\right|. \tag{7}$$

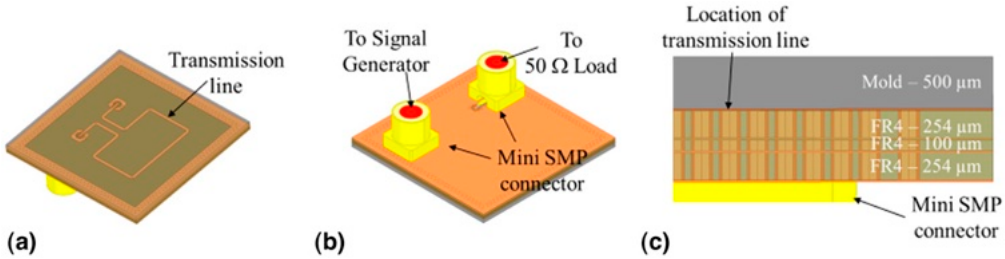

Fig. 2. Overview of DUT. (a) Transmission line on the top layer of PCB. (b) The bottom layer of PCB with Mini SMP connectors. (c) Stack-up of the DUT.

Hence, the total S.E. of a metal coating is composed of

$$\text{S.E.}\ (\text{dB}) = A\ (\text{dB}) + R\ (\text{dB}) + M\ (\text{dB}) \tag{8}$$

B. Measurement Setup

For the characterization of the package-level S.E., a device under test (DUT) is developed consisting of a four-layer PCB which is covered with an EMC as can be seen in Fig. 2. The EMC acts as a base for the application of the shielding material, i.e., sputter stacks of SuS/Cu/SuS with .18/3.80/.18 and 2/4/2 µm layer thicknesses as the state-of-the-art reference to compare against silver in various thicknesses applied by inkjet printing. This methodology to assess the S.E. of metal coatings has successfully been used in previous studies [7, 10, 11].

The DUT size is 20 × 20 mm^2. On the PCB's top layer, a 50 Ω transmission line is placed as a radiating source (Fig. 2a). This transmission line is connected by through-hole vias to the bottom layer of the PCB, where two Mini sub miniature push-on ((SMP)) connectors are mounted (Fig. 2b). One connector is used to interface to an excitation source, whereas the second is terminated by 50 Ω. The two inner layers of the PCB are reference planes for the transmission line and the connector section, respectively. By applying ground vias, any resonances between the reference planes are suppressed. In addition, leaking fields at the PCB's edges can be prevented.

To measure the S.E., the magnetic field radiated by shielded and unshielded DUTs is analyzed by applying a near-field scanning system as shown in Fig. 3. The setup consists of a DUT holder, a probe positioning system, where the magnetic field probe is located, and a signal generator as well as a spectrum analyzer which can create and capture RF signals at least up to 6 GHz. Due to the relation

$$\text{S.E.} = 20\ \log\frac{H(\boldsymbol{r})}{H^{'}(\boldsymbol{r})}, \tag{9}$$

where $H(\boldsymbol{r})$ and $H^{'}(\boldsymbol{r})$ are the measured magnetic fields of the unshielded and shielded DUTs at a specific location $\boldsymbol{r}$, a quick estimation of the S.E. properties can be carried out. In the current study, the probe always stays at the center of the DUT when the S.E. is determined.

Initial S.E. measurements on the sputtered reference samples with increasing distance between the probe and sample surface (z-direction sweep) result in two opposite trends (Fig. 4). For higher frequencies >4.5 GHz, the S.E. decreases with an increasing probe-to-surface distance, which is understood upon significant backside radiation originated from leakage at the SMP connectors on the sample backside (Fig. 4a). Accordingly, x/y position sweeps indicate symmetrical S.E. drop toward the DUTs edge if the probe is moved symmetrically on x-direction with respect to the placement of the SMP connector on the sample backside (Fig. 4b). If the probe is closer to the DUT edge adjacent to the SMP connectors monitored within a y-sweep (Fig. 4c), an asymmetric drop in S.E. indicates a stronger interference coming from the radiation leakage at the respective connector. These measurements are performed at a constant z-distance of 3 mm. Accordingly, proximity between the probe and sample surface results in a shadowing, that reduces bias effects from backscattering radiation originating from the SMP connectors.

The S.E., however, reaches a maximum at a probe distance of 3 mm for low frequencies ≤4.5 GHz (Fig. 4a), which has been described earlier as increasingly pronounced geometrical sensitivity based on mechanical artifacts with influences on the relative orientation between probe and sample surface changes in the angle of the incoming wave with respect to the probe surface [11]. Consequently, all S.E. values were extracted by a probe distance of 3 mm for $f \leq 4.5$ GHz, to minimize artifacts of geometrical factors, and the biased backscattering at 6 GHz is corrected upon using the S.E. at a probe distance of 1 mm.

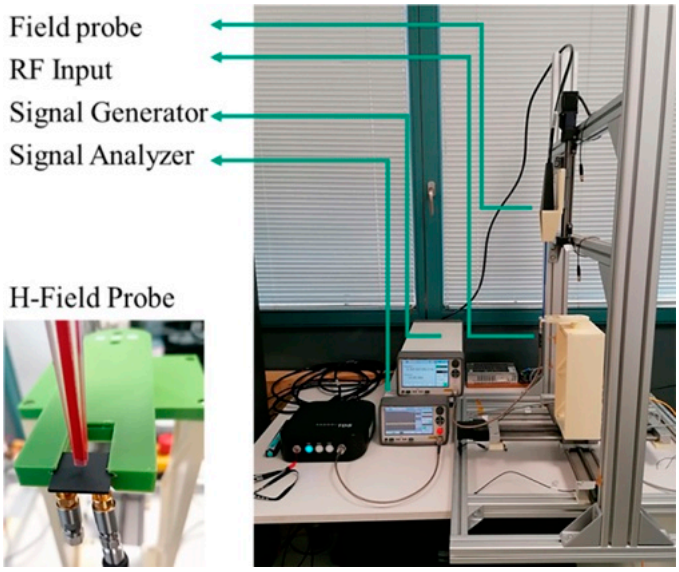

Fig. 3. Near-field measurement setup for magnetic field S.E. evaluation.

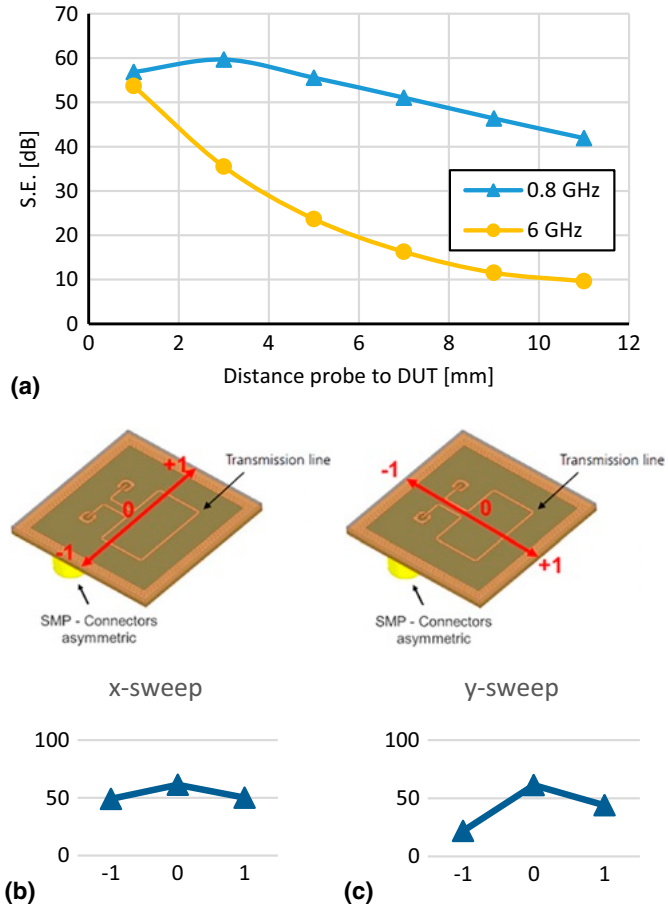

Fig. 4. Overview of probe distance characteristics. (a) Dependency of S.E. on probe distance for two frequencies. (b) Symmetric x-sweep with respect to the position of Mini-SMP connectors. (c) Asymmetric y-sweep with lower S.E. at position with close probe proximity to SMP connector.

C. Characterization of Ag Coating Layers

Within the Prexonics® System solution, a new technology for EMI shielding layer application is combining the advantageous particle-free MOD silver ink and a Heraeus inkjet printer for EMI shielding using maskless selective coating. It offers a perfectly matched solution comprising silver ink, printing/curing processes, and application equipment to create the optimal conductive coating, providing design flexibility for varied pattern layouts. Nonselective material deposition methods, such as plating, spray, or sputter technologies, achieve selective layer application only by masking/taping techniques. In contrast, the precise application of silver layers on the desired position on the five sides of a package (2.5D topology) allows for well-tailored shielding layer designs. This enables inserting trenches, stand-off coatings, or further surface features, such as laser markings and QR codes, and encourages to inspire package designers to elaborate beyond today's design rules, simply by changing the digital printing picture. Additionally, the inkjet printing technology further allows for the scalability of sample production from R&D trials, over fast prototyping, small scale, and full continuous productions on scalable equipment covering the whole spectrum of sample preparation in a cost-efficient manner.

The MOD ink technology itself is based on a fully dissolved silver precursor in a nonpolar solvent system that ensures superior open times of several weeks on the printer (floor-live) and offers outstanding stability (shelf-live) to enable transfer into mass manufacturing using uncritical chemistry without the requirements for special working environments (ATEX, etc.). The industrial scale inkjet printer is equipped with a specifically designed processor that translates the CAD coating drawing into accurate selectively coated components, which are processed in magazines of 300 mm ring carriers on which the components to coat are placed. All process steps are automated and inline: surface pretreatment via atmospheric plasma process, inkjet printing of the MOD metal ink, and sintering to a metallic coating film. Therefore, we designed an outstanding printing device to ensure stable printing conditions with technology-leading printing accuracy ready for light-off factory manufacturing as single workstation equipment to be implemented into the full continuous wafer manufacturing process for the semiconductor industry. The tool fulfills the standards of the semiconductor industry, and its mass-production capability has been proven.

The DUTs to investigate package-level shielding performance were conformally coated using Heraeus Prexonics® MOD inks upon the addition of more ink layers calculated for 208 nm silver per layer to build up a series of samples differing for their respective average layer thickness. The ink was cured using a UV curing profile of 120 s at a maximum temperature of 180°C full inline to result in finalized silver coating layers showing an average conductivity (sheet resistance) of 17% $\sigma(Ag_{Bulk})$ (bulk silver conductivity) determined by four-point probe measurements (Fig. 5).

At low coating thicknesses, an increase in relative conductivity with respect to $\sigma(Ag_{Bulk})$ indicates an incomplete sintering stage of the thin layers, that becomes constant at layer thicknesses of a minimum of 1.64 µm, which represents the thinnest layer for full interpretation within the course of this study. Thicker layers further exhibit the expected trend of decreasing sheet- and contact resistance with the coating layer thickness. The contact resistance determined as electrical resistance between the sample backside (grounding) and the center position of the top of the coating reflects the sheet resistance trend from the four-point probe measurement and serves as a

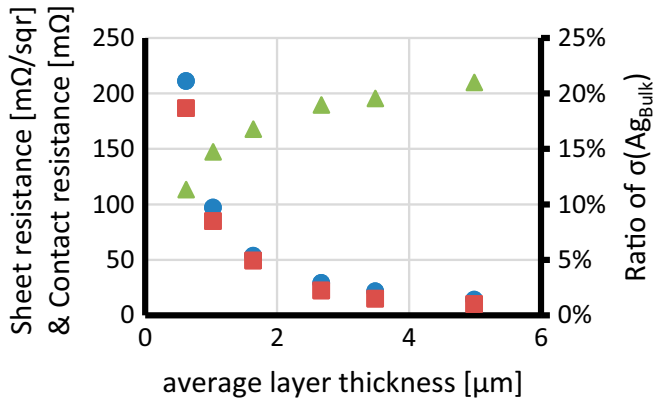

Fig. 5. Dependency of electrical performance (sheet resistance [blue], contact resistance [red], and bulk of Ag conductivity [green]) on layers thickness.

suitable characteristic to describe the electric performance of the sintered Ag coating. Measurements have been repeated four times per sample over two individual samples per coating thickness, respectively. Contact resistance measurements have been conducted using the four-terminal sensing method on an inductance/capacity/resistance (LCR) bridge from Rhode und Schwarz, sheet resistance was determined using a four-point probe on a device made by Ossila according to ASTM F390.

The layer thickness homogeneity was further characterized by x-ray fluorescence measurement based on the signal intensity from silver on EMC and externally referenced by a signal-to-thickness correlation derived by cross-section and microscopy analysis.

The position-dependent coating thickness over the sample surface (Fig. 6) does not indicate any accumulation of silver at certain remarkable positions (e.g., center), but indicates a random distribution over the whole sample surface.

A detailed distribution analysis (Table I) shows that all sample thickness measurements on the top side match well with the target. However, the significant standard deviation over all nine positions within two individual samples indicates inhomogeneous layer distribution, which is further reflected by the large total deviation

$$\text{Deviation} = \frac{t_{\max} - t_{\min}}{2 * t_{\text{average}}}. \tag{8}$$

A distinct layer thickness validation via microscopic studies on samples prepared from cross-section allows for rationalizing the unevenness of the surface thickness (Fig. 7).

The silver ink is initially following the conditions given by the substrate surface topology, and fluid properties will accordingly fill out the valleys on the top side, leaving a lower coverage on the summits of individual grain tips (Fig. 7, center). Note that all filler particles indicated as spherical gray structures are covered by epoxy resin on the top side. However, EMC-free grains are found at the sample sidewalls (Fig. 7, left). Accordingly, the side wall topology exhibits an even stronger expressed waviness as compared with the top side, and ink distribution is more driven by gap-filling-based forces on the ink surface tension at the sample side wall, than gravity as on the sample top side. If large grains are present on the sidewall surface, a low coating thickness results in the outer position of the resulting grain, and a larger thickness results vice versa at the position of pitch between grain and EMC.

The overall surface coating thickness is highly dependent on the individual measured spot and therefore only average values

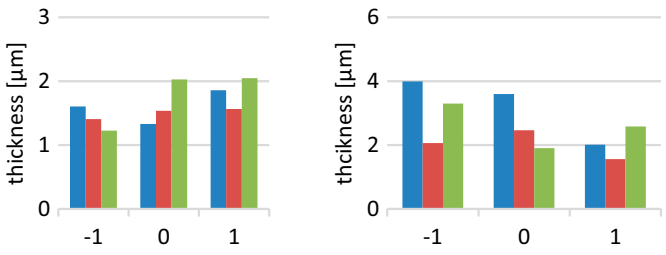

Fig. 6. Position-dependent Ag layer thickness mapping over the package surface by x-ray fluorescence analysis for a target layer thickness of 1.64 µm (left) and 2.67 µm (right).

Table I
Extracted Average Coating Thickness Compared with Target Thickness on Sample Top Side

	Unit	Sample	
Target thickness	[µm]	1.640	2.670
Measured average thickness on top side	[µm]	1.622	2.607
Standard deviation	[µm]	.279	.792
Deviation	[%]	25	47

give a reliable indication of the coating layer quality from inkjet printing and are well in line with the observed match in average thickness. Accordingly, average values, such as thickness over the full-substrate surface, or electrical conductivity are much better-suited measures to describe the coating layer's characteristics.

Comparison of the average layer thickness on the top side-to-side wall results in an average aspect ratio of 1.27 for 1.64 µm coating thickness and 1.36 for 2.67 µm, respectively. Sample preparation for this study focused on conformal package coating and did not emphasize the importance of a distinct top side-to-side wall aspect ratio. However, digital inkjet printing allows for individual treatment of each package layer even in the conditions of mass manufacturing equipment, and the results clearly indicate no limitations on certain maximum coating ratios, but full design freedom.

D. Characterization of Ag Coating S.E.

The S.E. trend of Ag-coated transmission line packages indicates a linear dependency on the frequency (logarithmic, Fig. 8). There is a significant difference between both investigated coating layer thicknesses of 2.67 and 1.64 µm, i.e., particularly observable at low frequencies. At higher frequencies ≥2.4 GHz, all shielding values are well above medium shielding levels of 40 dB, and differences in total shielding are within the error within the sample campaign.

An interpolated line indicates predictable shielding trends that allow for interpolation within the measured frequency range. There is an unexpectedly low shielding performance found for all samples at 1 GHz, which indicates weaker shielding than at an even lower frequency of 800 MHz, which contrasts with common shielding theory. However, shielding values at both low-end frequencies are within the error deviation and no systematic trend is assumed.

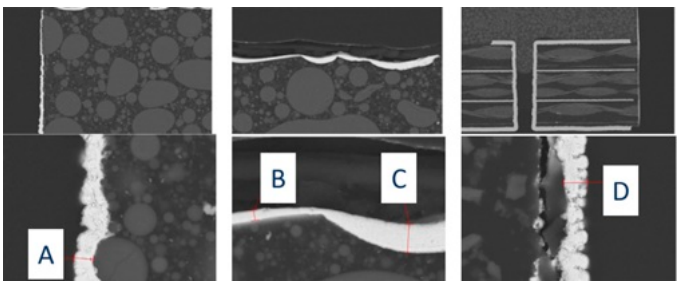

Fig. 7. Microscopy analysis after sample preparation via a cross-section of the sample with an average thickness of 2.67 µm (at the sidewalls [left and right], and the top side [center]). Selective thickness measurements are given at representative spots A = 2.1 µm, B = 1.1 µm, C = 3.1 µm, and D = 2.6 µm.

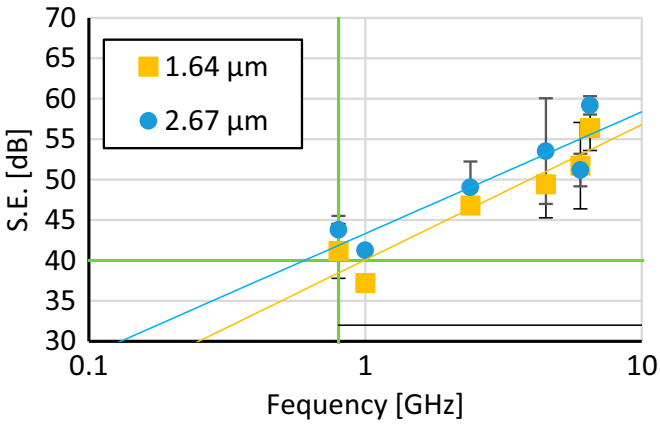

Fig. 8. Magnetic S.E. of Ag-coated samples with an average layer thickness of 1.64 µm (yellow) and 2.67 µm (blue) as a function of the incoming wave frequency and measured at a distance of 3 mm ($f \leq 4.5$ GHz) and 1 mm ($f > 4.5$ GHz) respectively. The green lines mark typical specifications of S.E. = 40 dB at f_{min} = 800 MHz.

Typical shielding requirements define an overall S.E. at minimum frequencies of 800 MHz to at least 40 dB, as indicated by the green lines (Fig. 8).

Commonly, S.E. is evaluated as a function of layer thickness. The data in the section "Characterization of Ag Coating Layers" indicate that the inkjet-printed layers exhibit an increased variation in thickness which does not affect the shielding capabilities. Hence, alternatively, the S.E. can be correlated with the respective contact resistance as a more reliable average characteristic of the silver coating (Fig. 9).

Accordingly, the ideal average coating thickness to achieve these requirements is between 1.64 and 2.67 µm, and contact resistance specifications indicate an ideal performance for the respective package design of 35 mΩ.

E. Comparison with Cu State-of-the-Art

Finally, the DUT of the current study was applied to the standard EMI shielding coating with standard sputter application parameters and addressed for layer thicknesses of SuS/Cu/SuS .18/3.80/.18 µm and 2/4/2 µm. Fig. 10 displays the results of the S.E. evaluation, in direct comparison with the

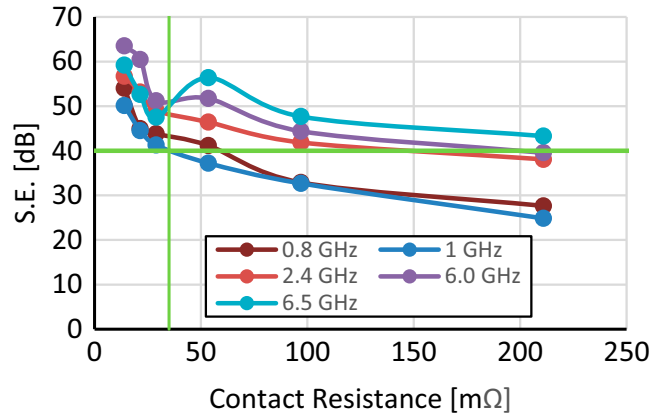

Fig. 9. Dependency of S.E. on the contact resistance of the coating layers and typical specifications at 40 dB and 800 MHz (green lines).

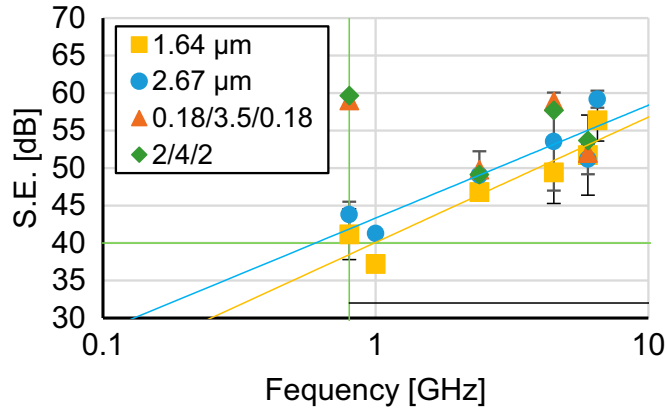

Fig. 10. S.E. of sputtered samples with layer stacks of SuS/Cu/SuS in two stack thickness variants and Ag layers over the frequency.

performance of Ag layers from inkjet printing. The mean S.E. measures identically for both surface stack variants within the standard deviation of both samples with max/min values of 60 dB at 800 MHz and 49 dB at 2.4 GHz. The total S.E. does not indicate a dependency on the respective frequency. The difference in shielding performance for the two coating variants is minor and only observable for the low-frequency range.

From the application point of view, there is no significant difference in the shielding performance between silver coatings (selectively applied via inkjet printing of particle-free MOD silver inks), and conformal coatings of three-layer stacks via sputtering technology at frequencies of ≥2.4 GHz. A tradeoff in shielding performance is only observable for low-frequency magnetic shielding; however, sputtering is exceeding typical requirements by factors and thus indicates an oversizing of the package coating with the potential to save time and material/energy for shielding layer production.

At high frequencies, absorption terms for total S.E. become the dominant shielding mechanisms. Accordingly, already thin layers provide sufficient shielding, as the skin penetration depth δ is thin compared with the coating thickness, as δ decreases with increasing frequency (eq. (1)). The overall impact of the shielding layer thickness becomes neglectable.

With decreasing frequency, the reflection term becomes the dominant contribution to the overall shielding mechanism, and differences between the two materials Cu and Ag get small. The residual incoming magnetic field can then only be attenuated via the absorption mechanism. At these low frequencies, the δ is within the thickness variations of shielding layers covered within this study. Accordingly, more radiation is attenuated by thick Cu as compared with significantly thinner Ag, on the top side of the sample and the difference in shielding layer coating thickness is reflected in the reduced shielding performance for the Ag-coated samples.

Conclusions

In summary, EMI shielding properties of thin silver layers applied by selective inkjet printing from particle-free MOD inks have been determined on specifically designed transmission line packages and compared against state-of-the-art shielding layer stacks of SuS/Cu/SuS 2/4/2 µm and .18/3.80/.18 µm. The results

indicate a frequency-independent S.E. between 49 and 60 dB for all coating variants and indicate a minimal required coating thickness between 1.64 and 2.64 µm for Ag to achieve S.E. of ≥40 dB at frequencies of ≥800 MHz. While the coating displays distinct variation in thickness, this does not degrade the S.E. by any means.

In comparison, the state-of-the-art sputter coating technology exhibits a significant overachievement of typical S.E. specifications, which indicates a significant overcoating of the sample top-side. The respective electrical properties, i.e., contact resistance of standard sputter coatings represent the oversized performance, and thus do not serve as an appropriate measure to benchmark well-tailored shielding layers. In contrast, correlations on S.E. on contact resistance must be drawn for new packages, to ensure full usage of design freedom benefits.

Selective silver deposition via additively inkjet printing of particle-free MOD silver inks allows for breaking current design rules and establishing conformal coatings with adjustable aspect ratios of 1:1 or higher.

Typical quality inspection items like coating layers electrical conductivity derived from sputtered references with overcoated top side dimensioning are not suited to unleash the full performance and economical potential of new technologies. Redefinition of specification items to ensure mass-production quality requires extraction of the true needs of a well-tailored shielding layer.

References

[1] R. Tummala, *System on Package: Miniaturization of the Entire System.* McGraw-Hill Education, 2008.

[2] D. Manessis, L. Boettcher, S. Karaszkiewicz, A. Ostmann, R. Aschenbrenner, and K.D. Lang, "Chip embedding technology developments leading to the emergence of miniaturized system-in-packages," IEEE 18th European Microelectronics & Packaging Conference, pp. 1-8, Brighton, UK, 12-15 September 2011.

[3] K. Hollstein and K. Weide-Zaage, "Advances in packaging for emerging technologies," IEEE Pan Pacific Microelectronics Symposium, pp. 1-11, HI, USA, 10-13 February 2020.

[4] C.A. Riso, et al., "Advanced packaging roadmaps and government needs," Proceedings of the Government Microcircuit Applications and Critical Technology (GOMACTech), pp. 21-24, Miami, March 2022.

[5] T. Löher, D. Schütze, M. Spanier, A. Ostmann, and M. Schneider-Ramelow, "PCB embedding technology for the miniaturization of complex electronic systems," 2022 IEEE CPMT Symposium Japan (ICSJ), pp. 21-24, 2022, Kyoto, Japan, 09-11 November 2022.

[6] N. Kim, L.H. Li, S. Karikalan, R. Sharifi, and H. Kim, "Package-level electromagnetic interference analysis," IEEE 64th Electronic Components and Technology Conference, pp. 2119-2123, Orlando, 27-30 May 2014.

[7] J. Hoang, R. Darveaux, T. LoBianco, Y. Liu, and W. Nguyen, "Breakthrough packaging level shielding techniques and EMI effectiveness modeling and characterization," IEEE 66th Electronic Components and Technology Conference, pp. 1290-1296, Las Vegas, 31 May – 03 June 2016.

[8] B. Kim, H. Jeon, D. Park, G. Kim, N. Cho, and J. Khim, "EMI shielding leadless package solution for automotive," *Journal of Advanced Joining Processes*, Vol. 5, pp. 100102, 2022.

[9] M. Nagata, T. Miki, and N. Miura, "Physical attack protection techniques for IC chip level hardware security," *IEEE Transactions on Very Large Scale Integration (VLSI) Systems*, Vol. 30, pp. 5-14, 2022.

[10] N. Karim, J. Mao, and J. Fan, "Improving electromagnetic compatibility performance of packages and SiP modules using a conformal shielding solution," IEEE 2010 Asia-Pacific International Symposium on Electromagnetic Compatibility, Beijing, pp. 56-59, 2010.

[11] L. Ding, X.-C. Wei, Z.-Y. Tang, J. Wen, L. Gao, and R.X.-K. Gao, "Near-field scanning based shielding effectiveness analysis of system in package," *IEEE Transactions on Components, Packaging and Manufacturing Technology*, Vol. 11, pp. 1235-1242, 2021.